International Journal of Mechanical Sciences 113 (2016) 61–70

Contents lists available at ScienceDirect

International Journal of Mechanical Sciences

journal homepage: www.elsevier.com/locate/ijmecsci

Automatic design of sheet metal forming processes by "un-forming"

E.G. Loukaides *, J.M. Allwood

Department of Engineering, University of Cambridge, Trumpington Road, Cambridge CB2 1PZ, UK

ARTICLE INFO

Article history:
Received 25 January 2016
Received in revised form
5 April 2016
Accepted 20 April 2016
Available online 23 April 2016

ABSTRACT

Most sheet metal components are made by deep drawing, which requires expensive tooling. Although many new flexible forming processes have been invented, they have largely not had industrial application, so it would be valuable if intelligent means to design new processes existed. This has not previously been attempted, although there has been work to classify both products and processes and to define optimal forming processes. A body of work in garment production examines the optimal flattening of garments, starting from their final form on a human body, to deduce the best cutting pattern from flat fabric. This paper develops a related approach for the first time, "un-forming" sheet metal from its finished geometry to a flat blank without prior specification of a process. An algorithm is developed that allows specification of process constraints and great freedom in implementing un-forming strategies, leading to a prediction of the strain history of the un-forming process. Reversing the direction of this history, allows prediction of the stresses in the workpiece required to form the target part, by use of an appropriate material model. The external forces (boundary conditions) required to maintain equilibrium with this stress state can then be calculated, allowing an iterative refinement of the constraints on un-forming until a physically achievable process has been designed. The approach is validated against a known process, and used to demonstrate how several previously untried forming strategies could lead to specification of new process designs. In future work, the method could be extended to allow an iterative specification of tooling to create the required boundary conditions, and hence to complete automatic process designs.

1. Introduction

Sheet metal components are ubiquitous, but options to produce them are relatively limited. Existing mass production processes such as deep drawing are inflexible, and consequently expensive for small batch, high-value production. In addition it takes time to produce and set up the required tooling. Furthermore, given the mechanics of these processes, half of all sheet metal never makes it into a product, having been cut off during manufacturing [1].

There has been great interest in the invention and exploration of flexible processes for the past 30 years, aiming to automate the skills of the craftsmen of earlier times. However, this has proved challenging: automated design of toolpaths for spinning remains elusive [2]; incremental sheet forming is limited by poor accuracy and high residual stress [3]; other novel processes have not flourished outside laboratory conditions. Thorough reviews of flexible forming processes are given by Jeswiet et al. [4], Allwood and Utsunomiya [5] and Groche [6].

Innovations in the technology of flexible metal forming have to date arisen either from the product of laborious experimental study or out of isolated eureka moments. Is it possible to design processes automatically? Surveys in the literature can be used to map available processes and identify gaps. Similarly, the literature can inform some design choices, but it does not provide means to design future machines for particular forming requirements. This paper therefore asks whether, rather than relying on accidents of innovation, structured means could be developed to design new sheet metal forming processes to meet customers' needs.

2. Literature review

Automatic design of new processes has not previously been attempted, but several strands of literature provide a foundation for work in this area. These include work on the classification of processes and products, the design of cutting patterns for garments, design of optimised blanks in deep drawing and the specification of criteria for optimal forming. These are briefly reviewed in turn.

The German DIN standard [7] presents a widely used classification of known processes to facilitate selection. Allwood [8] built on this aiming to envisage every possible configuration of tooling around a roll bite in ring rolling, inspired by Zwicky's idea [9] of

* Corresponding author.

http://dx.doi.org/10.1016/j.ijmecsci.2016.04.008

Nomenclature

$\bar{\sigma}$	Flow stress
σ_y	Yield strength – a material parameter
n	Material strain hardening parameter
$\bar{\epsilon}$	Equivalent plastic strain
W	Plastic work on workpiece
f,0 (subscripts)	Final and initial respectively
r (superscript)	Step in iteration for estimating formed part plastic strains
t_k (superscript)	Time step in un-forming procedure
dV	Volume of one element
ϵ_h	Natural plastic strain on edge i
e_{xx}, e_{yy}, e_{xy}	Cartesian plastic strains
x_j	Cartesian coordinates for node j
T_e	"Strain gauge rosette" transformation tensor
v,Q_v	Vertex and set of neighbouring vertices
S_v, R_v	Sets of vectors characterising the orientation of elements around vertex v
P	Set of nodes on the periphery of the workpiece
σ'_{ij}	Deviatoric stresses
λ	Plastic parameter

the morphological box. This was extended in a subsequent paper [10] to create a structured map of all possible configurations of any tools around any workpiece. However, although this appears exhaustive, the approach gives no insight into process mechanics and hence the feasibility of the different configurations.

Several authors have classified part geometry with the intention of automating the selection of process routes for different parts. Lie et al. [11] present an automatic feature extraction system for prismatic raw materials. Nasr and Kamrani [12] also attempt to automate feature recognition in an effort to bridge design and manufacturing. Similarly Li et al. [13] focuses on parts from the aviation industry, but extends existing feature recognition to consider a holistic attribute adjacency graph (HAAG). In future work part classification of this type could be used to allow the design of a forming process to create a family of parts, but the work in this paper will be restricted to creating a single target geometry.

Modelling the manufacturing process in reverse has created widespread interest in academic literature related to the garment industry, where complex final surfaces are defined by the body shape for which the garment is designed. Starting from this final target shape, the challenge for garment manufacturing is to design the cutting patterns leading to minimum waste of material and easy garment assembly. Several attempts have been made to develop algorithms which "un-form" the final garment into several flat components, using the locations of highest strain to optimise the pattern of cuts in the initial sheets of fabric. Early examples of these approaches are reviewed by McCarteney et al. [14], and more recently in Wang et al. [15]. A simplified mass-spring system is commonly used to model the 3D surface, with a subsequent optimisation that minimises the elastic energy, distances between nodes or the change in local area. This approach is similar to the challenge addressed in this paper, but differs in two key respects: the model of fabric deformation assumes elastic behaviour, where sheet forming must be plastic; the final garment is assembled from several components, where the ambition of this paper is to design the process for forming a single component.

A body of work related to this problem in the garment industry, the parameterisation of 3D surfaces to a 2D plane is a distinct field of research in applied mathematics with applications in cartography and computer graphics among others. Although this multidisciplinary interest in parameterisation has led to a large number of computational tools, most of them are not concerned with material bodies, hence do not produce physically realistic "flattenings" as shown by Hinds [16]. Azariadis and Aspragathos [17] and later Azariadis et al. [18], present some of the early ideas in computational parameterisation for 3D surfaces. They discretised the surface and flattened individual elements, allowing gaps to form between them, while later bridging those gaps using a geometric objective. However, their approach has no material model, aiming instead to minimise an overall metric of element distortion, so this cannot be translated directly to metal forming.

Within the literature of metal forming, inverse Finite Elements Methods have been used for various processes, but mainly for blank design in deep drawing: given a target product geometry, and hence tool shape, what shape should be cut from flat sheet (the blank) prior to forming? Lee and Huh [19] use an inverse method to produce blank shapes by minimising the plastic deformation energy, based on Hencky's deformation theory and Hill's anisotropic yield criterion. Cai et al. [20] used deformation non-uniformity as an objective function, along with volume constancy, aiming to minimise material waste. The initialisation of the simulation happens by moving all the nodes towards the target plane, which can cause numerical difficulties when analysing complex shapes. This approach relates to the ambition of this paper, but can only be used for a pre-defined process – which thus constrains the boundary conditions on the deformation of the workpiece.

One final area of literature relevant to the ambition of process design is the work by Chung and Richmond [21,22] aiming to specify the characteristics of optimal forming processes, defined as those which minimise the work of deformation across the workpiece. Under broad assumptions, they demonstrate that the deformation path of minimum work is one which has minimum effective strain across the workpiece. A practical implication of this insight is that by minimising the plastic work of deformation, the likelihood of failure for a given part geometry is reduced. However, to date, this approach has not been used for process design.

This review has demonstrated several strands of work that provide building blocks of knowledge towards an algorithm for designing sheet metal forming processes. Prior work on process classification has demonstrated the scope for innovation, but not addressed the physical constraints of deformation. Work on garment flattening and surface parameterisation was the inspiration for this paper, but in contrast to the approaches reviewed above, a non-linear model of material behaviour must be used throughout the deformation, to design a realistic sheet forming process. The geometrical and material nonlinearities of metal forming prevent development of exact analytical models and render existing computational methods (such as the ubiquitous finite element method) too slow for solving such a loosely constrained inverse problem. However, the definition of optimal forming can be applied to find optimal inverse (or "un-forming") processes (with minimum effective strain) subject to appropriate constraints, and the stress history of the reverse of this (the proposed forming process) then found from a suitable finite element model. The ambition of this paper is thus to assemble these component methods for the first time to explore process design by optimally "un-forming" a final part to an unspecified flat blank, without prior specification of the process.

3. Proposed new method for process design by "un-forming"

The algorithm proposed in this paper is summarised in Fig. 1: a target part is optimally "un-formed" (measured by the integral of total effective strain over the workpiece) to a flat blank, subject to kinematic constraints. An initial set of constraints is used to specify a "forming strategy" (such as incrementally reducing the curvature of the part, or specifying a direction of motion for the part perimeter) and these constraints are iteratively refined based on predictions of the boundary conditions that must be applied to the workpiece during forming. An additional set of constraints is used to prescribe desired deformation characteristic (such as pure shear deformation).

The method shown in Fig. 1 is iterative: for some set of process constraints, a target part is optimally "un-formed" to a flat blank; the deformation history of this un-forming is then reversed to calculate the strain and stress histories of the forwards forming process that would form the target part from the calculated flank blank. From these stresses, the boundary conditions required to establish equilibrium are calculated. A user can then examine the feasibility of applying these boundary conditions and iteratively refine the constraints applied to the next un-forming calculation. The feasibility potential can be assessed by the strains involved in the deformation and the external load required to produce them. When the resulting deformation is revealed to be infeasible, the original un-forming strategy and assumptions are amended and the process is repeated, until a feasible deformation path is found. Further details of these two stages of the calculation follow in the next two sections.

3.1. Optimally un-forming a target part subject to constraints

The algorithm of Fig. 1 could be used for any achievable target part geometry, but in this paper only a square cup shape is considered, shown in Fig. 2. This geometry was chosen, based on the part classification work of [23] since it contains both developable and non-developable regions, as well as flanging. Furthermore, a process that achieves this geometry locally can potentially achieve similar or increasingly complicated shapes by superposing appropriate toolpaths. The cup is 40 mm deep with a total width of 120 mm. The rim on each side is 10 mm wide. A triangular mesh is created on this part – also shown in Fig. 2 – to allow for discretization of the constraints and the objective function that follow. It is assumed that the process has sufficient symmetry that only one quarter of the square cup need be analysed in the simulation, in order to reduce computational time.

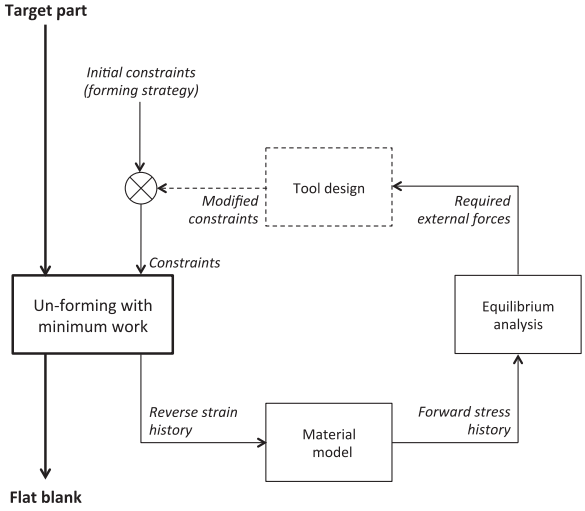

Fig. 1. Block diagram showing the basic steps in the suggested method. (Dashed lines indicate stages of the algorithm currently performed manually.).

The un-forming optimisation algorithm minimises the plastic work done, W, on the entire domain of the workpiece, Ω, at each step of un-forming. The nodal coordinates are represented by x. Chung and Richmond [21,22] call this "ideal forming" since, under certain conditions, it distributes deformation across the workpiece so that deformation before failure is maximised. Thus the objective function maximises the feasible deformation *globally*.

Specifically, the objective function f is defined as:

$$\arg\min_{x\in\Omega} f = \sum_{i=1}^{m} dW_i \tag{1}$$

$$\text{subject to } A_i^{t_k} = A_i^{t_0},\ \forall\ i\in\Omega \tag{2}$$

$$x_p^{t_k} = C,\ \forall\ \in\omega,\ \omega\in\Omega \tag{3}$$

and to symmetry conditions across the x and y-axis. Here, m is the number of elements in the mesh. The area of element i is A_i while the superscripts indicate the time steps; for each element the area at any time step is constrained to remain equal to its initial area. For any sheet material discretised in two dimensions and under the constant volume hypothesis for plastic deformation of metals, this implies that there is no change in thickness or equivalently that the deformation is in pure shear. The variables in the optimisation are the Cartesian coordinates of all the nodes in the mesh, since they are the basis for calculating both the plastic work decrement and the updated areas of the elements. The additional kinematic constraints applied in each method are described separately in each relevant section below, and are similarly defined in the code in terms of the nodal coordinates. They are noted above in a generic form with the second constraint.

The plastic work in each element, at each step, is given [24] as:

$$dW = \bar{\sigma} d\bar{\epsilon} dV \tag{4}$$

where $\bar{\sigma}$ is the flow stress, $d\bar{\epsilon}$ is the equivalent plastic strain decrement and dV is the element volume. The minimisation occurs after each displacement controlled step mentioned in the constraints above.

The elements are treated as constant strain triangles and an equivalent plastic strain decrement for each element can be calculated at each step using the natural strain on each element edge:

$$\epsilon_h^{t_k} = \ln\left(\left\| x_j^{t_k} - x_k^{t_k} \right\|_2 / \left\| x_j^{t_{k-1}} - x_k^{t_{k-1}} \right\|_2 \right) \tag{5}$$

where x_j and x_k are the node coordinates that define edge h of each element. The three strains are combined in one vector $\epsilon^{t_k} = [\epsilon_1^{t_k}, \epsilon_2^{t_k}, \epsilon_3^{t_k}]$. Effectively, the 2D element does not account for bending energy, but given the required large changes in Gaussian curvature for general un-forming, stretching energy is expected to dominate. From these strains their Cartesian counterparts for each element, i, are obtained:

$$de_i^{t_k} = \begin{bmatrix} de_{xx} \\ de_{yy} \\ 2de_{xy} \end{bmatrix} = T_e \epsilon^{t_k} \tag{6}$$

with

$$T_e = \begin{bmatrix} c_1^2 & s_1^2 & s_1 c_1 \\ c_2^2 & s_2^2 & s_2 c_2 \\ c_3^2 & s_3^2 & s_3 c_3 \end{bmatrix} \tag{7}$$

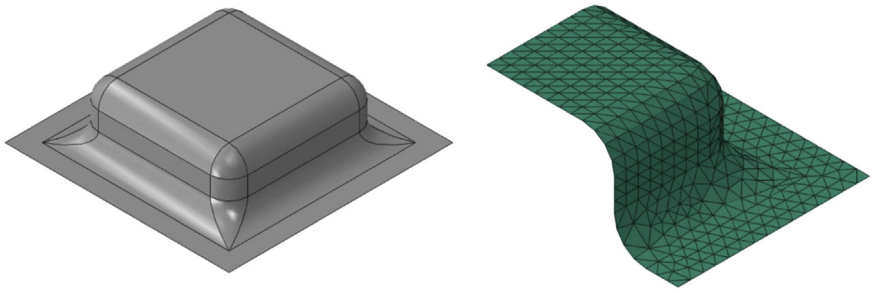

Fig. 2. The square cup geometry used in the examples, along with a meshed counterpart taking advantage of the double symmetry.

the "strain gauge rosette" transformation tensor. Here, c and s are sines and cosines of the element angles to a local Cartesian coordinate system in the plane of the element. The node coordinates are transformed to this local system.

The equivalent plastic strain decrement for the element is given by these Cartesian strains as:

$$d\bar{\epsilon}_i=\sqrt{\frac{2}{3}\left[\left(de_{xx}\right)^2+\left(de_{yy}\right)^2+2\left(de_{xy}\right)^2\right]} \tag{8}$$

The strain hardening material law is given by

$$\bar{\sigma}=\sigma_y(0.05+\bar{\epsilon})^n \tag{9}$$

where, as above, $\bar{\sigma}$ is the flow stress and $\bar{\epsilon}$ is the equivalent accumulated plastic strain.

In the examples, the material parameters, σ_y and n, were defined for aluminium 1100-O as 172 MPa and 0.25 respectively, based on values taken from [25], and adapted to exclude the elastic region. The form of Eq. (9) maintains the same values for σ_y and n as the referenced source. Effectively, only the plastic strains are taken into account since they are assumed to be much greater than the elastic strains. Currently the method employs an isotropic model, but with some additional work, the formulation can include anisotropic materials.

Substituting Eqs. (8) and (9) in Eq. (4), and summing over all elements as per Eq. (1), the plastic work required at the current step can be calculated and thus it can be supplied to the optimizer. Both the optimisation process and the inclusion of constraints – in these examples the constant area constraint – are performed via the well-known 'fmincon' function with the 'interior-point' algorithm in MATLAB [26–28]. Specifically, the 'interior-point' algorithm runs until an objective function tolerance is achieved, or the variable tolerance is reached, etc. MATLAB documentation explains additional stopping criteria. Table 1 gives the options chosen for 'fmincon'.

The optimal decrement is subtracted from the total effective strain at each step:

$$\bar{\epsilon}^{t_k}=\bar{\epsilon}^{t_{k-1}}-d\bar{\epsilon}^{t_{k-1}} \tag{10}$$

After each step the resulting nodal coordinates are saved for post-processing. The cumulative equivalent plastic strain is also saved to be used in the next optimisation step. The flow stress at each step, and for each triangle is also calculated based on the equivalent plastic strain estimate.

3.1.1. Estimating the initial plastic strains

Since the part is un-formed, the accumulated plastic strain at the start of the calculation above, must be initialised at some value, such that after it has decreased during un-forming, the final flat workpiece has no plastic strain. To initiate the calculation this trial value of accumulated plastic strain must be estimated. Hence, the assumption is made that for any forming operation in this context, the flat blank has no initial plastic strains. But for the starting formed part in the un-forming method, the plastic strains need to be estimated. This estimate is obtained with the following iterative method: The simulation is initialised with a value of $\bar{\epsilon}=\bar{\epsilon}_0^{(1)}=0.5$ throughout the workpiece. The un-forming strategy is followed to completion and the final equivalent plastic strains on the flat workpiece are recorded. The final $\bar{\epsilon}_f$ improves the initial guess by using:

$$\bar{\epsilon}_0^{(r)}=\bar{\epsilon}_0^{(r-1)}-\bar{\epsilon}_f^{(r-1)} \tag{11}$$

with r being the current step in the iteration. The process is repeated using the updated initial plastic strain. After a limited set of steps, a mean final strain is obtained that is sufficiently close to zero, allowing for the initial strain field to be verified. To facilitate this, the material law is slightly adapted to ensure only positive values of $\bar{\epsilon}_E$ are used:

$$\bar{\sigma}=\sigma_y(0.05+\max\{\bar{\epsilon},0\})^n \tag{12}$$

This modification prevents unphysical negative equivalent strains from affecting the result and encourages convergence of the iteration.

Table 1
Options given to fmincon.

	Value
MaxFunEvals	1e8
TolCon	1e−3
TolFun	2e−1
TolX	1e−6
MaxIter	1e5

3.2. Iteratively refining the process constraints

Once the optimisation algorithm has completed, to create a flat workpiece, a complete history of displacement in un-forming has been established, so this can now be reversed and considered to be the history of forming the part from the blank. For each displacement controlled forwards step, an incremental strain field can be calculated by comparing nodal coordinates for successive time steps, as defined in Eq. (10). A stress field can then be produced through the flow rule $de_{ij}=\lambda\sigma'_{ij}$, where σ'_{ij} represents the deviatoric stresses and λ is the plastic parameter given from the flow stress curve as:

$$\lambda=\frac{3d\bar{\epsilon}}{2\bar{\sigma}}=\frac{3d\bar{\epsilon}}{2\sigma_y\bar{\epsilon}^n} \tag{13}$$

thus giving the deviatoric stresses,

$$\sigma'_{ij}=\frac{2de_{ij}\sigma_0\bar{\epsilon}^n}{3d\bar{\epsilon}} \tag{14}$$

In order to calculate the full stress field on the workpiece, which also allows for the evaluation of external forces needed for the obtained deformation, an elastoplastic material model is essential. It can be easily obtained by setting up a displacement controlled model in a Finite Element package.

The method of Fig. 1 allows for constraints to be used to impose chosen characteristics on the process. These constraints may include requirements for the workpiece, an overall forming strategy, and limits on boundary conditions (particularly the definition of areas without applied tools, where equilibrium must be maintained within the workpiece).

Constraints on the workpiece may include forming limits, or other preferences on deformation. For example, in this work a pure shear deformation has been imposed, to maintain uniform part thickness. Such uniformity would be attractive in many applications, and is to a large extent a characteristic of some existing sheet processes, such as spinning [24]. There is also some experimental evidence that forming in pure shear allows for the maximum local deformation before failure; Forming Limit Diagrams show no established failure boundary in the pure shear direction [29]. In this model, this constraint is enforced by ensuring the area of mesh elements remains unchanged during deformation. The pure shear constraint maximises the feasible deformation *locally* while, as previously explained, the objective function maximises the feasible deformation *globally*.

Kinematic constraints may be applied to define an overall strategy by which the target part is un-formed to flat. Many approaches could be used, and in the next section, three strategies are presented and explained in detail. In general, a forming strategy is given by applying displacement control to certain nodes at each time step, with a subsequent relaxation/optimisation step. With a high number of such steps, a smooth deformation history can be ensured, while relatively small strain decrements are needed in each step.

Constraints on boundary tractions can be imposed as functions of the geometry of deformation, for example to impose the requirement that some areas of the workpiece are not in contact with any tools. The deviatoric stress field can be used to inform the necessary features of the process tooling, since the literature provides a variety of examples of known tooling force profiles. But the deviatoric stresses do not provide the full required stress state. To obtain that, the resulting deformation can be reversed and used for a displacement controlled FE simulation thus producing the full nodal force field required. Given the full nodal deformation field, there is a unique solution to this problem, which well-established FE software, such as Abaqus, can provide. Once the required external forces are observed adjustments can be made to the initial constraints.

In summary, the novel proposal of Fig. 1 is to translate the algorithm used by McCartney [14] for garments to metal forming, allowing for many un-forming strategies, and for a range of process constraints. The next section demonstrates this algorithm in practice.

4. Design of a test case and various un-forming strategies

The algorithm developed in the previous section is first validated against a mature application, and then used to demonstrate three different strategies for designing a process to create the target part shown in Fig. 2.

4.1. Validation case

In this section the reliability of the method is demonstrated via comparison with a shear test. The test setup is emulating similar experiments usually constructed to test material properties, see for example [30]. In this experiment, a disk of 30 mm radius, which is clamped at the centre, up to a radius of 15 mm, has its outside perimeter rotated gradually. The same experiment is attempted on the Abaqus FE package so as to produce a starting mesh for the un-forming strategy. The material properties in Abaqus are the same as mentioned above, but with an elastic component allowed. In Abaqus, the elastic deformation of the elements is the basis for calculating the hydrostatic stresses, which in turn are required to ensure equilibrium. The material is given a Young's modulus of 71 GPa, a Poisson's ratio of 0.33 while the plastic behaviour is provided in tabular form to match the power law parameters given previously.

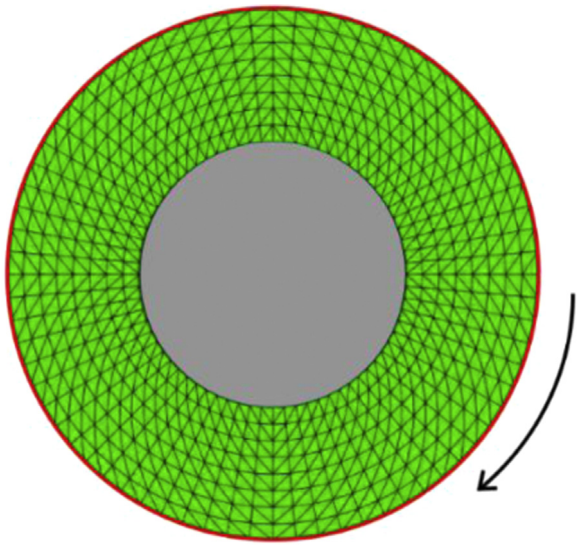

Fig. 3. The method is tested by a pure shear 2D setup, where an annulus is clamped in the middle and rotated at the external perimeter (shown in red). The initial mesh used in Abaqus is shown here. (For interpretation of the references to colour in this figure legend, the reader is referred to the web version of this article.).

A triangular mesh of 1760 elements to describe the annulus, while the clamped region is excluded since the inner perimeter nodes are fixed, but allowed to rotate. The FE model uses S3R shell elements and a single static implicit step to apply a $\pi/30$ clockwise rotation on the external perimeter – a shown in Fig. 3. A relaxation step follows where the outer radius boundary condition is removed to allow any elastic effects to dissipate. The resulting deformed mesh is then used as the starting point of an un-forming process using an un-forming algorithm.

The MATLAB optimisation here works by excluding the inner and outer nodes from the objective function and the constraints. Instead they are given prescribed values at each of one of 5 steps used. In the case of the inner nodes, they stay fixed at their initial locations while the external nodes rotate by $\pi/150$ rad anticlockwise at each step. At each step, the optimizer is first given the zero objective function so that a feasible "initial guess" location for the remaining nodes is generated. This is followed by the optimisation of the plastic work while maintaining the constant area constraint. A comparison between the Abaqus results and the results of the presented method is shown in the next section.

4.2. Un-forming via local flattening of high Gaussian curvature regions

The kinematic constraints described above, can be used to impose a strategy of successive local flattening on the path to the un-formed blank. Analysis of the spinning process has demonstrated that deformation in near to pure shear conditions can be

achieved by a single working tool if the workpiece has a saddle shaped geometry. This allows the creation of tension in one direction and compression in the other within the workpiece. The strategy presented in this section therefore preferentially flattens the regions of the workpiece with the most negative Gaussian Curvature.

In order to locate the vertex of highest negative Gaussian Curvature the 'patchcurvature' function [31] is used. This calculates the Gaussian Curvature at each vertex by performing a least-squares fit of a quadratic patch to the neighbourhood of each vertex. The formulation takes into account up to second-degree neighbours of each vertex. The algorithm does not revisit any vertex and eventually regions of negative Gaussian Curvature are exhausted. The method proceeds by visiting the vertex of most negative Gaussian Curvature that has not been flattened already.

Once a vertex, v, is chosen, its neighbours are discovered and the vectors connecting the neighbours to v, Q_v are then projected onto the tangent plane to the workpiece at v. This action is followed by an optimisation step with a zero objective function, where 'fmincon' attempts to find a feasible solution which conserves area and achieves pure shear as described previously. In a subsequent optimisation step, the usual objective function for plastic energy is resumed and a co-planarity constraint is placed on v and its neighbouring vertices. Specifically, the cross product of adjacent vectors in the set Q_v is calculated, producing a second set of vectors, P_v, which corresponds to the normal vectors on all triangular elements that contain v. Then, the cross product of adjacent vectors in P_v is calculated, and norms of resulting vectors are stored in vector R_v and added to the 'fmincon' equality constraints as:

$$R_v=0, \tag{15}$$

thus requiring that all normal vectors in P_v are parallel, or that all points in the set $\{v,Q_v\}$ are coplanar. The constraint is applied to every v already flattened, i.e. an attempt is made to keep previously flattened regions flat, as well as flattening the current region.

4.3. Un-forming via radial boundary pull

An alternative inspiration for a forming strategy is found the familiar process of deep drawing. In deep drawing, the boundaries of the blank move towards the deeper locations on the die. During un-forming, the blank boundaries are therefore moving outwards. Thus, in this case, displacement control is applied on the peripheral nodes during un-forming so that they move along a linear trajectory pointing radially outwards from the axis of symmetry of the square cup.

The "bottom" of the cup is assumed to remain flat, and this region is used to define the orientation of the target plane for the flattening. Hence, the trajectory of the periphery nodes ends on that plane. From the earlier assumption of a radial path each is placed on a line, but to find their exact location, one more assumption is made: the final arc length of the workpiece along radial lines is the same at the beginning and end of the simulation.

The diagram in Fig. 4 shows the trajectory of a single node starting at point A on the original periphery of the part and moving towards point B such that the radial distance from the node to the part's centre, O, along the surface, stays the same. This trajectory is given to all peripheral nodes with a corresponding end point to conserve their respective radial arc distance (although the Figure only displays one for clarity of presentation). One hundred time steps are used in the simulation, with all the periphery nodes moving $1/100^{th}$ of the distance from A to B on each one. This is reflected in an additional equality constraint to

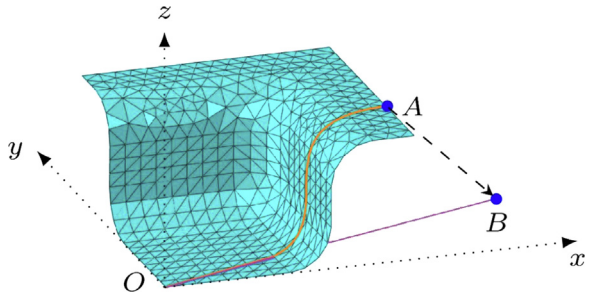

Fig. 4. The linear trajectory of a single peripheral node is shown here as a dashed line (AB) with B residing on the xy plane. The initial arc length (orange) is the same as the target final radial distance from the origin (purple). The xz and yz planes define planes of symmetry. (For interpretation of the references to colour in this figure legend, the reader is referred to the web version of this article.).

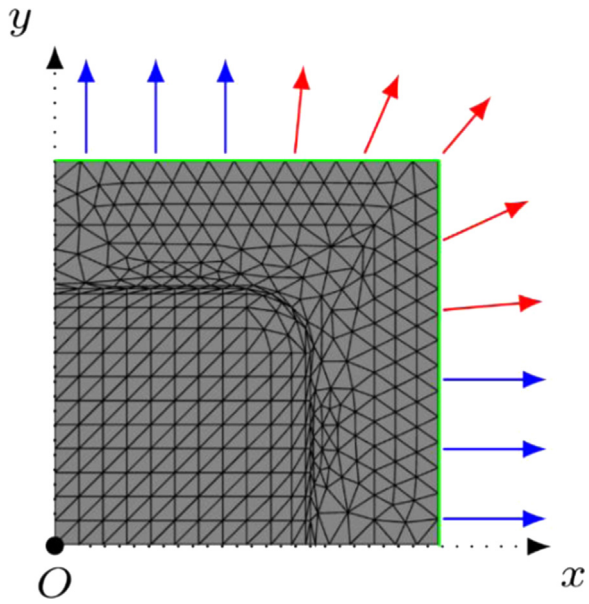

Fig. 5. In this strategy, part of the periphery is prescribed a radial trajectory (red), while other nodes move in parallel where the part is developable (blue). The trajectory has a vertical component not shown here. (For interpretation of the references to colour in this figure legend, the reader is referred to the web version of this article.).

'fmincon' that requires that all peripheral nodes are in the vicinity of these prescribed locations, or:

$$x_j^{tk}-y_j^{tk}=0,\ \forall\ j\in P \tag{16}$$

Where x are the coordinates of mesh vertices, y are points on linear trajectories described above, and P is the set of peripheral vertices on the brim of the workpiece.

The same diagram also more clearly shows the target plane for the flattening, Oxy, that coincides with the flat region at the centre of the cup. This plane, along with its normal vector at O, also serves as the global Cartesian coordinate system. All nodes that begin on the symmetry planes Oyz and Oxz must remain on the planes.

4.4. Un-forming via variable boundary pull

From deep drawing, and from the geometry of the part, an alternative deformation path at the boundary can be imagined. Although the corners of the square cup must be stretched, the central region of its sides could be un-formed by bending alone. Hence, instead of the radially outward motion described in the

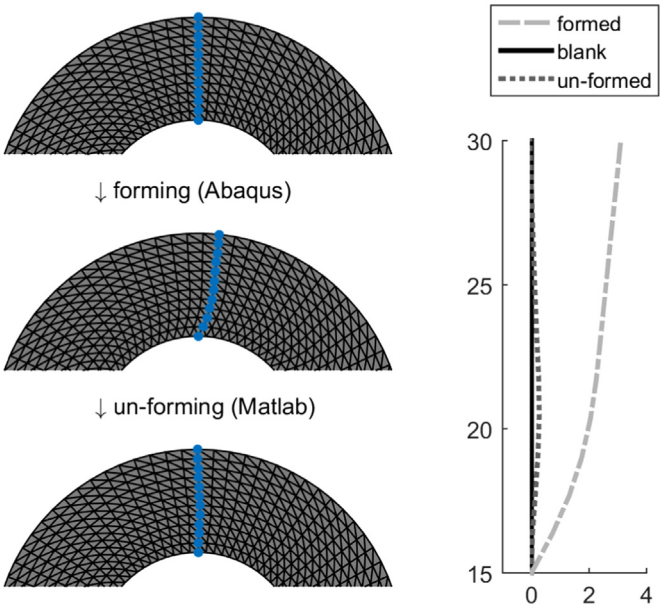

Fig. 6. The method is validated by un-forming the resulting mesh of a pure shear test in Abaqus. On the left the initial, the formed and the un-formed mesh are shown from top to bottom. Similarly the locations of one set of radial nodes is marked on the meshes and shown in detail on the right.

previous section, an alternative approach to un-forming is to prescribe radial motion to the corner section, and sideways motion to the central section of the periphery.

In more detail, and if the perimeter nodes on the side parallel to the x-axis are used as an example: the section starting at the y-axis and ending at the centre of that edge are move along a trajectory parallel to the y-axis. The section from the centre of the edge to the corner of the workpiece, is given a radial trajectory, identical to the trajectory described in the previous section. In both cases, the end of the trajectory aims to maintain the corresponding length of the workpiece.

This is displayed in Fig. 5 where a plan view of the initial mesh is shown. The periphery nodes are marked in green and the trajectories of the two actuated sections – the developable and the non-developable – are shown in blue and red respectively.

5. Results

Each simulation produces the geometry of the mesh at each step, which can be reversed and animated to illustrate the deformation path of the candidate new process. As previous work has focused on the blank shape that can be inferred from flattening, a corresponding shape is found at the end of each simulation here.

Once the geometry of the mesh at each step has been obtained, strain and stress fields are produced following the method of Section 3. The strain field is visualised by plotting vectors representing the principal strains on each element. The results for the forming strategies discussed above are shown in this section, but first the validation of the method through the test case example is given.

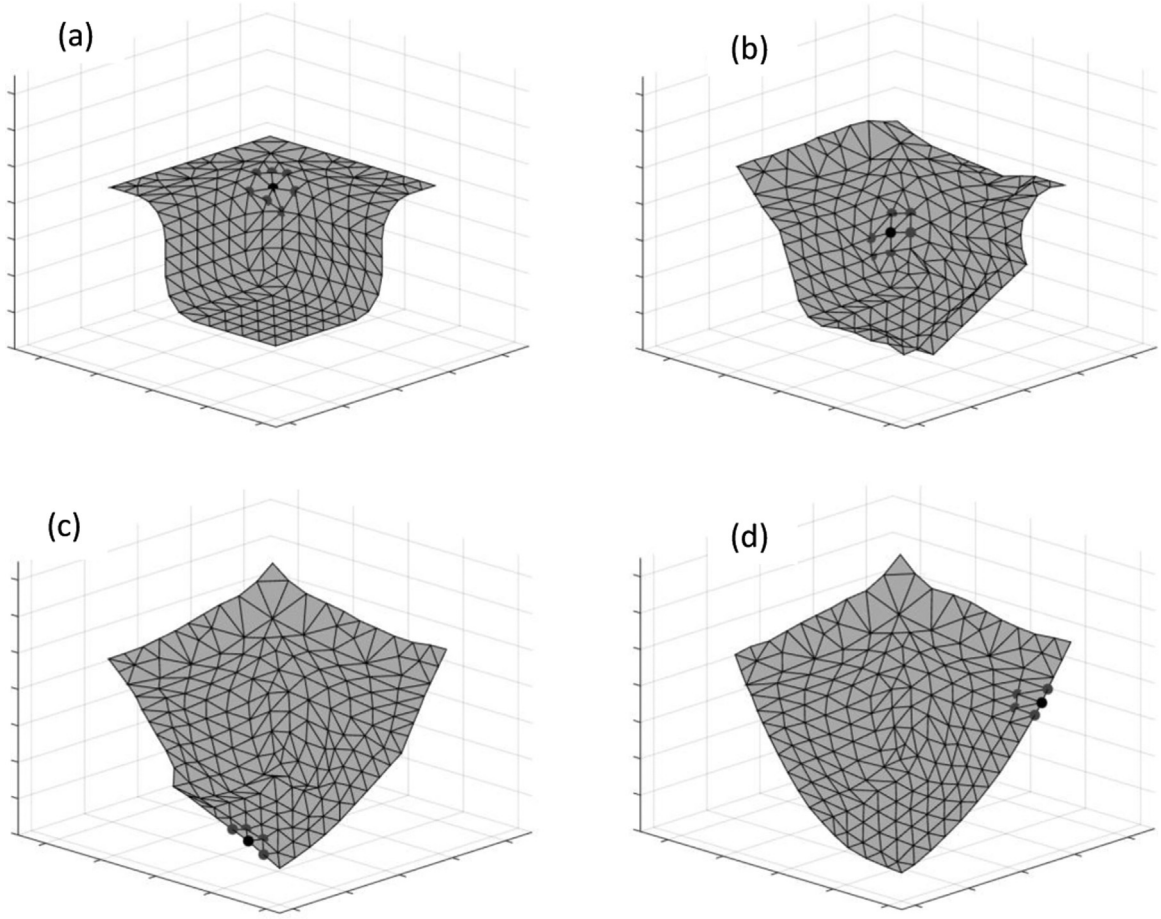

Fig. 7. Progress of the increasing GC local flattening method. The black dot and the grey dots represent the node currently being flattened along with its neighbours.

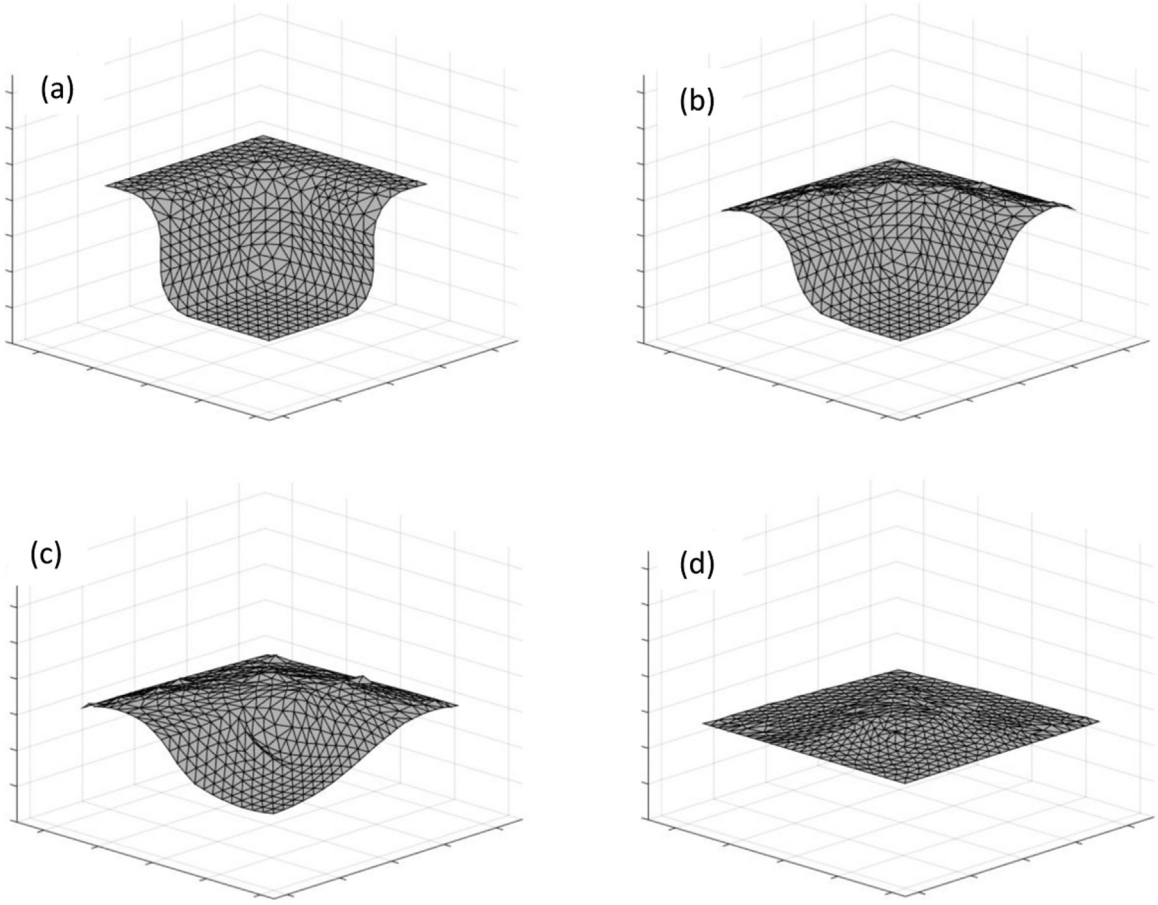

Fig. 8. The deformation path for the radial boundary pull strategy. Frames 2, 58, 98 and 130 are shown.

5.1. Test case results

In Fig. 6 the method is validated through the shear test described in Section 4. On the left diagram the initial mesh is shown at the top. The results of a 'forming' operation in Abaqus are shown below that, during which a $\pi/30$ rotation of the external perimeter prescribed. This deformed mesh then serves as the initial geometry for an un-forming operation. On the right, the relative locations for one set of radial nodes are shown. The same set of nodes is marked on the meshes on the left. The optimisation approach results are a close match to the initial mesh. Any discrepancies can be attributed to the elastoplastic nature of the material defined in the FE package, while the plastic work approach discards the elastic components of strain. It is also noted that for the modelling of pure shear close-to-equilateral triangles present better results, and large distortions of elements could further explain minor discrepancies.

5.2. Results for un-forming via highest negative GC

The deformation trend is presented in Fig. 7, where few frames from the output (specifically frames 2, 102, 202 and 302 out of 302) are shown. The node currently being flattened in each frame is marked with a black dot, along with its neighbours in grey. This method succeeds in gradually reducing the magnitude of Gaussian Curvature across the workpiece but fails to find a continuous deformation path to the global flattened state: the end point of this strategy is the smooth 'bowl' shape in Fig. 7(d).

The algorithm using this forming strategy was computationally expensive, since to maintain the co-planarity constraint, a number of matrix operations must be performed at each iteration of the optimisation. Perhaps for the same reason, 'fmincon' frequently reaches an infeasible solution. This result also prevented the iterative process to estimate the initial equivalent plastic strain field.

5.3. Results for un-forming via radial boundary pull

This strategy provides deformation data that are more applicable to a process design. "Pulling" the periphery of the cup along a linear trajectory forces the rest of the workpiece to deform in a smooth and controlled manner. The resulting stages of deformation are shown in Fig. 8. The algorithm does not run to completion since the required pull at the periphery needed to produce the flat shape is less than the length of the trajectory described in the method. Instead, by step 65 out of 100, which corresponds to frame 130, all nodes are within 3 mm of each other in the z-direction. This plane is not the xy plane, but instead a parallel plane above it; during the deformation, the centre of the workpiece slowly rises. The method notably produces the most complete unforming and the most intuitive intermediate geometries.

The effective plastic strain for each element is calculated from Eqn (10) and shown in Fig. 9 (left). The results are shown halfway through the flattening process – i.e. at frame 66. In this example, the greatest deformation occurs where the brim of the cup meets the corners. The regions in the deeper part of the cup remain mostly unaffected during this stage of the deformation.

For some elements, the effective strains are potentially exceeding the ultimate strain for the material defined here. This would indicate that given the chosen constraints the process is not

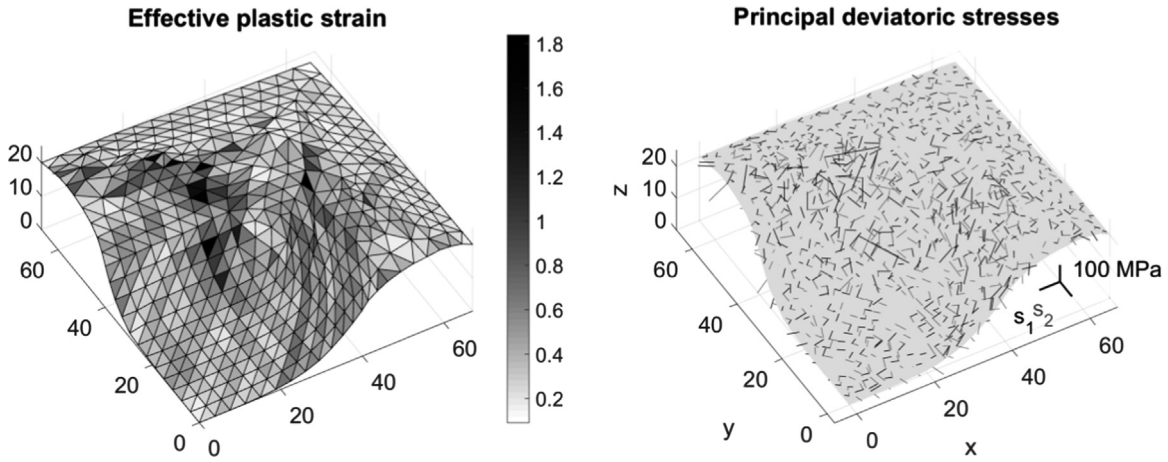

Fig. 9. On the left, the effective plastic strain at each element is plotted halfway through the simulation. The large strains indicate that for such a deep part, the constraints imposed to the process are not viable. On the right, the principal deviatoric stresses are shown with blank and grey segments for the same step, and for each element.

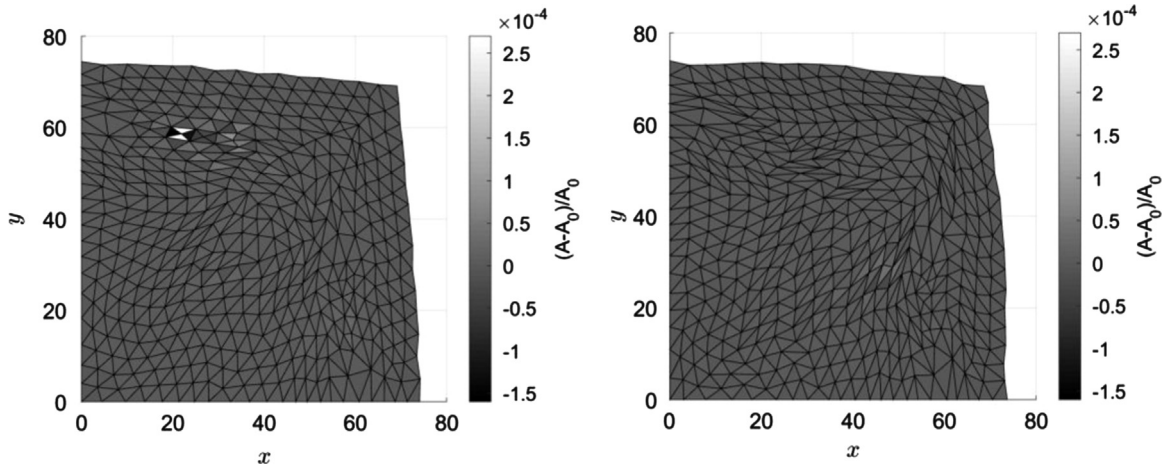

Fig. 10. Plan view of the final step in the optimisation using both the radial boundary pull (left) and the variable boundary pull (right). The colour map shows the relative change in area for each element.

applicable to the specific part. A more complicated kinematic strategy could dissolve the concentration of strains in particular locations.

Similarly the deviatoric stresses are calculated using Eq. (14) and also plotted in Fig. 9 (right). Again, this is useful in observing the relative stress state of elements or groups of elements and examining its feasibility.

5.4. Results for un-forming via variable boundary pull

As expected the results from this strategy are similar to the results in the previous section. In particular the stages of deformation are similar to the frames shown in Fig. 8 using the radial pull strategy, and hence are omitted. The final step is instead shown in Fig. 10 to allow direct comparison with the results of the previous section. The final perimeter differs slightly in the two cases but the relative change in area varies almost by an order of magnitude. The locations of maximum through-thickness strains in the two cases are similar, where developable and non-developable regions of the surface meet – see Section 4.4.

6. Discussion

This paper has made a first demonstration of the transfer of a technique from the garment industry to sheet metal forming. The approach allows un-forming to a flat blank, while minimising work and maintaining sheet thickness, and allows for any forming strategy, three of which have been demonstrated. The method produces strain fields which can be used to assess the feasibility of forming a part subject to specified process constraints and for given material parameters.

A wide range of forming strategies could be explored in future, including prescribed thickness variation for the workpiece. Similarly, un-forming can be instigated at different locations, as demonstrated in the Gaussian Curvature strategy, but could also focus on other metrics, for example increasing Mean Curvature.

In addition to the direct calculations on the elements above, it is also possible to use the deformation path of the mesh to produce the exact forces required on each node. This can be demonstrated through use of a standard FEM package, by setting up a displacement controlled simulation that corresponds to the results of the method of Section 3.1 with the displacements are provided in the forwards direction – from flat geometry to the final target part.

For example in Fig. 11, the halfway frame in the simulation is shown, with a profile view of the workpiece and the necessary nodal forces. The largest forces are needed in shaping the flange at this time step while the bottom and walls of the cup only require relatively small tool forces.

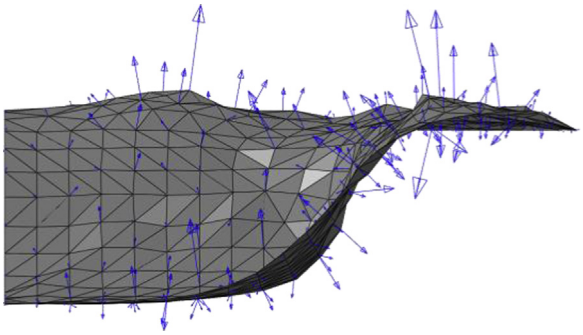

Fig. 11. A relative plot in profile view of nodal forces required halfway through the process to produce the desired deformation.

This work has presented a design strategy that can be employed for a variety of process constraints, and potentially to a wide array of challenging target parts. A general optimisation solver has been used in this work, but the method could be improved in future work with faster algorithms – see for example Raithatha [32]. The high variability in the direction of nodal forces in Fig. 11 is a consequence of the pure shear constraint imposed throughout this deformation. Future work will aim to reconcile the predicted forces to available tooling options, through iterative refinement of the process constraints to be more representative of the tractions that could be applied by real tools, as indicated in Fig. 1. This could include use of template forms of nodal force that could exist under a tool, and a clustering algorithm to classify regions of similar required forces.

Acknowledgements

This research was supported by the EPSRC Grant EP/K018108/1.

References

[1] Milford RL, Allwood JM, Cullen JM. Assessing the potential of yield improvements, through process scrap reduction, for energy and CO_2 abatement in the steel and aluminium sectors. Resour Conserv Recycl 2011;55(12):1185–95.
[2] Polyblank JA, Allwood JM. Parametric toolpath design in metal spinning. CIRP Ann Manuf Technol 2015;64(1):301–4.
[3] Allwood JM, King GPF, Duflou JR. A structured search for applications of the incremental sheet-forming process by product segmentation. Proc Inst Mech Eng Part B: J Eng Manuf 2005;219(2):239–44.
[4] Jeswiet J, Geiger M, Engel U, Kleiner M, Schikorra M, Duflou J, Neugebauer R, Bariani P, Bruschi S. Metal forming progress since 2000. CIRP J Manuf Sci Technol 2008;1(1):2–17.
[5] Allwood JM, Utsunomiya H. A survey of flexible forming processes in Japan. Int J Mach Tools Manuf 2006;46(15):1939–60.
[6] Groche P, Fritsche D, Tekkaya E a, Allwood JM, Hirt G, Neugebauer R. Incremental bulk metal forming. CIRP Ann Manuf Technol 2007;56(2):635–56.
[7] DIN8580, Manufacturing Processes – Term and Definitions. Deutches Institut Fur Normung E.V.: 2003.
[8] Allwood JM. A structured search for novel manufacturing processes leading to a periodic table of ring rolling machines. J Mech Des Trans ASME 2007;129(5):502–11.
[9] Zwicky F. Discovery, invention, research through the morphological approach. New York: McMillan; 1969.
[10] Allwood, JM. A structured search for new metal forming pro cesses. In: Proceedings of the international conference on technology of plasticity; vol. 2008: 2008. p. 1–6.
[11] Liu SC, Gonzalez M, Chen JG. Development of an automatic part feature extraction and classification system taking CAD data as input. Comput Ind 1996;29(3):137–50.
[12] Abouel Nasr ES, Kamrani AK. A new methodology for extracting manufacturing features from CAD system. Comput Ind Eng 2006;51(3):389–415.
[13] Li YG, Ding YF, Mou WP, Guo H. Feature recognition technology for aircraft structural parts based on a holistic attribute adjacency graph. Proc Inst Mech Eng Part B: J Eng Manuf 2010;224(2):271–8.
[14] McCartney J, Hinds BK, Seow BL. The flattening of triangulated surfaces incorporating darts and gussets. Comput Des 1999;31(4):249–60.
[15] Wang CCL, Smith SSF, Yuen MMF. Surface flattening based on energy model. CAD Comput Aided Des 2002;34(852):823–33.
[16] Hinds BK, McCartney J, Woods G. Pattern development for 3D surfaces. Comput Des 1991;23(8):583–92.
[17] Azariadis P, Aspragathos N. Design of plane developments of doubly curved surfaces. Comput Aided Des 1997;29(10):675–85.
[18] Azariadis PN, Nearchou AC, Aspragathos NA. An evolutionary algorithm for generating planar developments of arbitrarily curved surfaces. Comput Ind 2002;47(3):357–68.
[19] Lee CH, Huh H. Blank design and strain estimates for sheet metal forming processes by a finite element inverse approach with initial guess of linear deformation. J Mater Process Technol 1998;82(1–3):145–55.
[20] Cai Z-Y, Li M-Z, Zhang H-M. A simplified algorithm for planar development of 3D surface and its application in the blank design of sheet metal forming. Finite Elem Anal Des 2007;43(4):301–10.
[21] Chung K, Richmond O. Ideal forming – I. Homogeneous deformation with minimum plastic work. Int J Mech Sci 1992;34(7):575–91.
[22] Chung K, Richmond O. Ideal forming – II. Sheet forming with optimum deformation. Int J Mech Sci 1992;34(8):617–33.
[23] Kannan TR, Shunmugam MS. Processing of 3D sheet metal components in STEP AP-203 format. Part II: feature reasoning system. Int J Prod Res 2009;47(5):1287–308.
[24] Lange K. Handbook of metal forming. United States of America: McGraw-Hill; 1985.
[25] Hosford W, Caddell R. Metal forming: mechanics and metallurgy: 2011.
[26] Byrd RH, Hribar ME, Nocedal J. An interior point algorithm for large-scale nonlinear programming, vol. 9, no. 4: 1999 p. 877–900.
[27] Byrd H, Gilbert JC, Nocedal J. A trust region method based on interior point techniques for nonlinear programming. Math Program 2000;89:149–86.
[28] Waltz RA, Morales JL, Nocedal J, Orban D. An interior algorithm for nonlinear optimization that combines line search and trust region steps. Math Program 2006;107(3):391–408.
[29] Sheet metal forming: fundamentals. In: Altan T, Tekkaya AE, editors. ASM International; 2012.
[30] Yin Q, Tekkaya AE, Traphöner H. Determining cyclic flow curves using the in-plane torsion test. CIRP Ann Manuf Technol 2015;64(1):261–4.
[31] Kroon DJ. Patch Curvature: 2014.
[32] Raithatha A, Duncan SR. Rigid plastic model of incremental sheet deformation using second-order cone programming. Int J Numer Methods Eng 2009;78(8):955–79.